Highlights

A Patchwork Method to Improve the Performance of Current Methods for Solving the Inverse Problem of Electrocardiography

Oumayma Bouhamama,Mark Potse,Laura Bear,Lisl Weynans

- A novel ECGI approach is presented which combines classical methods to optimize the inverse solution.
- This Patchwork Method gives better results than the individual methods even in the presence of Gaussian signal noise.
- This is the first time ECGI validation has been performed using classical numerical approaches in the case of sinus rhythm.

A Patchwork Method to Improve the Performance of Current Methods for Solving the Inverse Problem of Electrocardiography

Oumayma Bouhamama[a,b,c], Mark Potse[a,b,c], Laura Bear[c,d,e,*,1] and Lisl Weynans[a,b,c,*,1]

[a]Université de Bordeaux, IMB, UMR5251, Bordeaux, France
[b]CARMEN team, Inria Bordeaux – Sud-Ouest, Bordeaux, France
[c]IHU-Liryc, Fondation Bordeaux Université, Bordeaux, France
[d]Université de Bordeaux, CRCTB, U1045, Bordeaux, France
[e]Inserm, U1045, CRCTB, France

ARTICLE INFO

Keywords:
inverse problem
patchwork method
method of fundamental solutions
finite element method
boundary element method
noninvasive electrocardiographic imaging
ECGI
electrocardiography

ABSTRACT

Background: Noninvasive electrocardiographic imaging (ECGI) provides panoramic images of cardiac electrical activity from potential measurements on the torso surface. However, current methods do not accurately reconstruct sinus rhythm, and in particular miss or misplace breakthrough sites.

Method: We propose a novel "patchwork method" (PM), which combines two classical numerical approaches for ECGI: the method of fundamental solutions (MFS) and the finite-element method (FEM). We assume that the method with the smallest residual in the predicted torso potentials provides the most accurate solution. These residuals were computed using the boundary-element method, and projected onto the heart surface using an orthogonal projection. The PM then selects for each heart node and each time step the method whose estimated reconstruction error is smallest. The performance of the PM was compared to both FEM and MFS alone using simulated ectopic and normal ventricular activation beats.

Results: Cardiac potentials and activation maps obtained with the PM (CC=0.63±0.004 and 0.61±0.05 respectively) were more accurate than MFS (CC=0.61± 0.005 and 0.48±0.05 respectively) or FEM (CC=0.58±0.009 and 0.51±0.02 respectively). The PM also succeeded in locating all epicardial activation breakthrough sites, whereas the individual numerical methods usually missed one. Moreover, the PM outperformed the other methods in the presence of Gaussian measurement noise added to the torso surface potential distribution, showing its robustness and stability with respect to noise.

Conclusions: The PM overcomes some of the limitations of classical numerical methods, improving the accuracy of mapping important features of activation during sinus rhythm and paced beats.

1. Introduction

The inverse problem of electrocardiography, also known as noninvasive electrocardiographic imaging (ECGI), combines electrical potential measurements on the torso surface with a geometric description of the heart and torso to reconstruct their cardiac source. Most ECGI approaches describe this cardiac source as the electrical potentials on the epicardial surface of the heart.

ECGI can help to diagnose and treat cardiac conditions. For example, ECGI has been demonstrated to help predict the benefit of cardiac resynchronization therapy [1, 2] and to detect ablation targets for atrial fibrillation [3]. However, recent clinical and experimental validation studies have shown that current clinical implementations of ECGI are inaccurate in reconstructing electrical activity in the presence of i) complex conduction patterns such as in sinus rhythm or in the presence of conduction block [4, 5], and ii) structural abnormalities [6]. That is, the detection of focal activity, and epicardial breakthrough sites can be missing or misplaced. The problem is seen not only with clinical data [5] but also in torso tank experiments where the forward model is well defined [1, 4], implying that the issue lies with the inverse methods themselves.

*Corresponding author
laura.bear@ihu-liryc.fr (L. Bear); lisl.weynans@math.u-bordeaux.fr (L. Weynans)
ORCID(s): 0000-0001-5855-5795 (O. Bouhamama); 0000-0003-4166-2687 (M. Potse); 0000-0002-7070-2492 (L. Bear)
[1]Co-last author

The objective for this study is therefore to improve the performance and the accuracy of ECGI in the reconstruction of focal activity, and epicardial breakthrough sites. We will achieve this by optimizing the reconstruction accuracy of current inverse methods in order to limit the numerical artifacts produced.

ECGI can be mathematically represented by the following Cauchy problem for the Laplace equation which relates the potential field on the heart surface Γ_h to the potential field on the torso surface Γ_T:

$$\begin{cases} \nabla \cdot (\sigma_T \nabla \Phi_T) = 0 & \text{in the torso volume} \\ \sigma_T \nabla \Phi_T \cdot n_T = 0 & \text{on } \Gamma_T, \\ \Phi_T = \Phi_h & \text{on } \Gamma_h, \end{cases} \tag{1}$$

where Φ_T is the potential field in the torso, Φ_h the potential field on the heart surface, σ_T the torso conductivity tensor field and n_T the outward normal direction. Several classic numerical methods have previously been proposed to solve this problem, including the boundary-element method (BEM) [7], the finite-element method (FEM) [8] and the method of fundamental solutions (MFS) [9]. Each of these methods reduces the governing equation (1) to a matrix-vector system describing the forward problem of electrocardiography:

$$\Phi_T = A\Phi_h, \tag{2}$$

where A is a transfer matrix, its form differing according to the numerical approach used. To recover the values of Φ_h from Φ_T, we can invert the linear system (2) to obtain

$$\Phi_h = A^{-1}\Phi_T. \tag{3}$$

This linear problem has a unique solution only if the number of measurements on the torso surface is larger than the number of values expected on the heart surface. But this is often not the case. Moreover, the inverse problem has an ill-posed nature, which means that even low levels of error in the model or noise in the potentials can cause large errors in the solution. The solution to both issues is to regularize the problem. The regularized problem will be well-posed, that is, will have a unique solution whose value is less influenced by the level of noise. Tikhonov regularization [10] is the most commonly used regularization method to solve this inverse problem. It minimizes the functional

$$F = \|A\Phi_h - \Phi_T\|_2^2 + \lambda_t^2 \|R\Phi_h\|_2^2, \tag{4}$$

where λ_t is a constant weighting term at time t controlling the level of regularization and R the regularization operator. The first term is the least squares solution to equation (2) and the second term defines a spatial constraint on the solution as a function of the choice of R.

To solve the inverse problem, equation (3) can be reduced using equation (4) to

$$\Phi_h = (A^T A + \lambda_t^2 I)^{-1} A^T \Phi_T. \tag{5}$$

Despite the large number of possible methods to solve the inverse problem of electrocardiography, no single algorithm consistently outperforms the rest. Previous studies comparing different methods have found that the optimal algorithm depends on the data set [11], the level of noise [12, 13] and the geometric error present in the data [13]. We therefore sought to combine these existing algorithms, to make the most of their advantages while minimizing their limitations. This Patchwork Method (PM), locally chooses the algorithm that provides the optimal solution, defined as the method that minimizes the estimated reconstruction error.

2. Methods

2.1. Current numerical methods

In this study, three classic numerical methods were used to solve (1) to obtain the transfer matrix A (equation 2): the FEM [8], the BEM [7] and the MFS [9]. All three methods used the same epicardial mesh to solve the inverse problem (5132 nodes and inter-node spacing 0.8 to 9.5 mm). At the torso surface, the MFS used a linear triangular surface mesh with 252 nodes located at typical electrode locations for clinical ECGI systems (inter-node spacing 22.6 to 218 mm) (Figure 1). The BEM used a more refined linear triangular torso surface mesh (1234 vertices and inter-node spacing 8.6 to 35.1 mm). The FEM used the same torso surface as the BEM, with the volume between the torso and heart surface discretized using tetrahedral elements to form a volumetric mesh (15788 nodes, inter-node spacing 0.1 to 110 mm) (Figure 2).

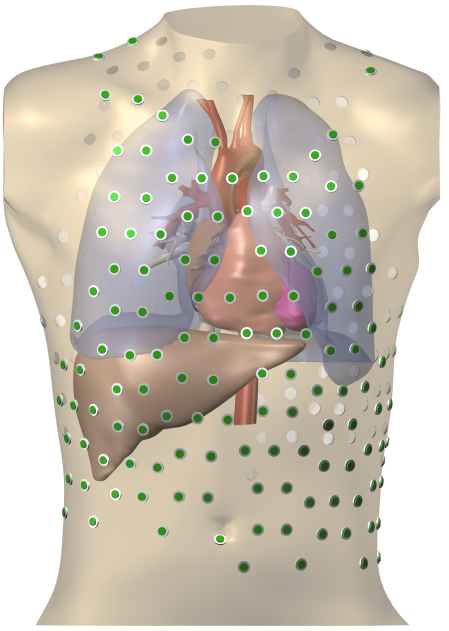

Figure 1: Segmented torso with internal organs and 252 torso electrode positions.

2.2. Patchwork Method

The linear relationship between the cardiac source and the torso surface potentials after discretization with any of the above-described methods can be written in matrix form:

$$A\Phi_{\mathrm{h}} = \Phi_{\mathrm{T}},$$

where A is the transfer matrix obtained using the different numerical methods, Φ_{T} the torso measurements and Φ_{h} represents either the potentials on the heart surface for the FEM or the BEM, or the coefficients of the linear combination of fundamentals solutions in the case of the MFS. We denote by A_{F}, A_{B} and A_{M} the transfer matrices for the FEM, BEM and MFS respectively.

Let Φ_{ex} be the exact solution. We assume that all numerical methods used for the computation of the transfer matrix are consistent with the forward problem of ECGI, meaning that the residual of Φ_{ex} tends to zero when the mesh size tends to zero:

$$\lim_{h\to 0} R_{\gamma}(\Phi_{\mathrm{ex}}) = 0, \ \gamma = F, B, M,$$

where the residuals, $R_{\gamma}(\Phi_{\mathrm{h}}) = A_{\gamma}\Phi_{\mathrm{h}} - \Phi_{\mathrm{T}}$ with $\gamma = F, B, M$, represent the difference between the numerical solution on the torso obtained with Φ_{h} and the measurements Φ_{T}. We propose to use this property as a criterion to select locally, among the inverse solutions obtained, the one that is closest to the exact solution, without knowing what the exact solution is.

For this study, we have compared the inverse solutions obtained with the FEM and MFS using zeroth-order Tikhonov regularization [10] and with the regularization parameter determined by the CRESO method [14]. Their residuals are then obtained using a BEM transfer matrix.

The PM algorithm is the following:

- For each time step n:
  - Compute the approximate potential values $\Phi^n_{\mathrm{h,F}}$ and $\Phi^n_{\mathrm{h,M}}$ obtained with the FEM and the MFS,
  - Use these values to compute the forward solution and the associated residuals $R_B(\Phi^n_{\mathrm{h,F}})$ and $R_{\mathrm{B}}(\Phi^n_{\mathrm{h,M}})$ on the torso surface using the BEM,

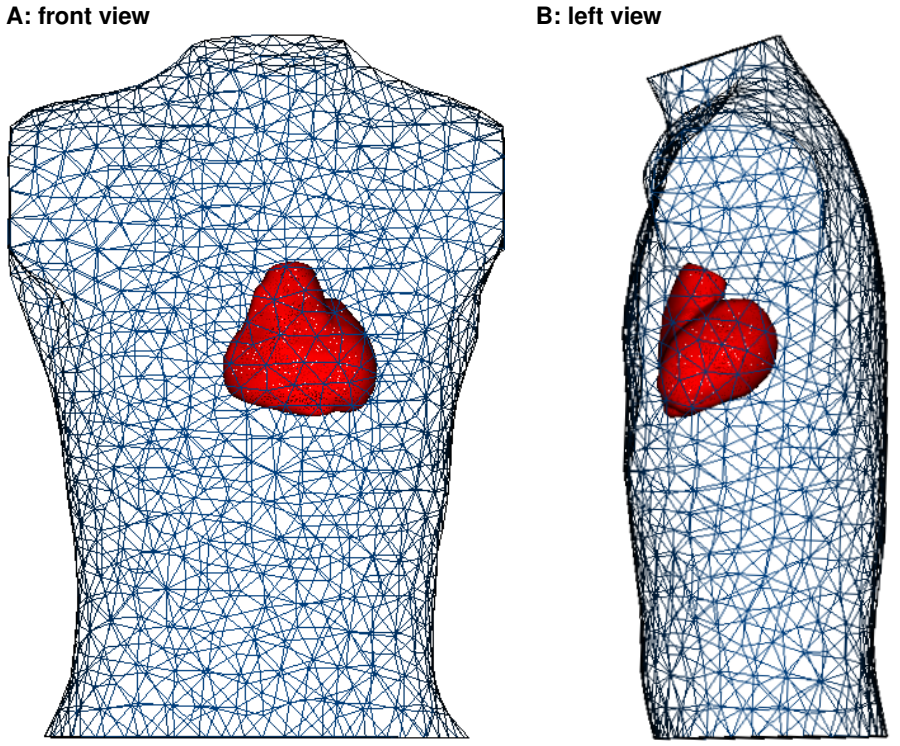

Figure 2: The heart-human-shaped torso tank model. The two views are from the front (A) and from the left side (B). The heart consisted of 5132 nodes and 10260 elements and the tank had 15788 nodes and 95975 tetrahedral elements

  - Project the residuals from the torso onto the heart surface using an orthogonal projection. The residual value of each node on the torso is assigned to the heart node closest to the projected torso node in the normal direction.
  - For each epicardial node, select the method whose residual is the smallest on the corresponding torso point, and define a coefficient $\alpha^n = 0$ if the MFS has the smallest residual, and 1 otherwise.

- Perform a temporal regularization of the coefficient α to avoid sudden variations between successive time steps:

$$\tilde{\alpha}^n = 0.025\,\alpha^{n-4} + 0.05\,\alpha^{n-3} + 0.1\,\alpha^{n-2} + 0.2\,\alpha^{n-1} + 0.25$$
$$\alpha^n + 0.2\,\alpha^{n+1} + 0.1\,\alpha^{n+2} + 0.05\,\alpha^{n+3} + 0.025\,\alpha^{n+4}$$

- For each time step n, compute the new approximate solution as

$$\Phi_{\mathrm{h}}^n = \tilde{\alpha}^n \Phi_{\mathrm{h,F}}^n + (1 - \tilde{\alpha}^n)\Phi_{\mathrm{h,M}}^n$$

2.3. Data

The methods were evaluated using data generated with a detailed heart-torso model that was previously tailored to a patient [15]. We used a set of 10 simulations of ventricular paced beats, and 8 simulations where Purkinje fibres were stimulated to replicate a sinus rhythm beat. Although the atria and sinus node are not included in these later simulations, we will from here refer to these as sinus rhythm.

Activation was simulated with a monodomain reaction-diffusion equation using the TNNP membrane model [16], on a hexahedral mesh with 0.2-mm resolution. Extracellular potentials were computed by solving the elliptic bidomain equation in a whole-torso model at 1-mm resolution [17]. Damage patterns consisted of sheets of connective tissue aligned with the 3 coordinate axes [18]. The sheets were 0.4 mm thick and were placed at 1-mm intervals. 20 % of the surface of the sheets consisted of randomly placed holes. The sheets extended through the entire myocardium but not

through the thin layer that represents the Purkinje system in the model. The stability and the robustness of the inverse approaches was tested by adding Gaussian measurement noise to the torso surface potentials at noise levels of 0.5%, 1% and 2% of the overall signal amplitude.

2.4. Evaluation Metrics

To quantify the accuracy of the inverse solutions, we computed the relative error (RE) and the correlation coefficients (CC) between the simulated "ground truth" and the reconstructed potentials as

$$RE = \sqrt{\frac{\sum_{i=1}^{N}(\Phi_i^{\mathrm{C}} - \Phi_i^{\mathrm{M}})^2}{\sum_{i=1}^{N}(\Phi_i^{\mathrm{M}})^2}} \tag{6}$$

and

$$CC = \frac{\sum_{i=1}^{N}(\Phi_i^{\mathrm{M}} - \bar{\Phi}^{\mathrm{M}})(\Phi_i^{\mathrm{C}} - \bar{\Phi}^{\mathrm{C}})}{\sqrt{\sum_{i=1}^{N}(\Phi_i^{\mathrm{M}} - \bar{\Phi}^{\mathrm{M}})^2}\sqrt{\sum_{i=1}^{N}(\Phi_i^{\mathrm{C}} - \bar{\Phi}^{\mathrm{C}})^2}} \tag{7}$$

where N is the number of epicardial nodes at which the cardiac potentials are simulated and reconstructed, Φ_i^{C} and Φ_i^{M} are the inverse-computed potential and the corresponding simulated potential respectively at epicardial node i, and $\bar{\Phi}^{\mathrm{C}}$ and $\bar{\Phi}^{M}$ are the spatial means of inverse-computed and simulated potentials, respectively.

Activation times were determined using a spatio-temporal algorithm developed for ECGI potentials [19]. For activation maps, the RE and CC were also computed between simulated and inverse-computed values.

Epicardial breakthrough sites were identified from activation maps as sites with local early activation. When activation was near simultaneous (<2 ms variation) over a large zone of tissue, the center of this area was taken as the breakthrough site. The localization error (LE) of these breakthrough sites was calculated using the geodesic distance, and the time difference (offset breakthrough) between the ECGI-detected and the nearest simulated breakthroughs was calculated.

Graphing and statistical analysis were performed using the statistics software GraphPad Prism 8.3. For each metric, the significance of the differences was tested using a repeated measures one-way ANOVA with inverse method, or two-way ANOVA with noise level and inverse method defined as the independent variables. $p < 0.05$ was defined as significant. Data are expressed as mean ± SD.

3. Results

3.1. Paced beats

Figure 3 shows examples of simulated and reconstructed electrograms during a paced beat captured at (A) late, (B) intermediate and (C) early activation sites. At each site, the optimal method selected by the PM is seen when the electrogram traces overlap. For these nodes the MFS was selected most often. However, for a few key time steps the FEM was selected as optimal, as is seen during the steep downslope in panel A. This resulted in a higher correlation of electrograms reconstructed with the PM compared to electrograms reconstructed with either the MFS or FEM alone.

Figure 4 shows a spatial map of the percentage of the electrogram that the PM selected from each method (FEM or MFS) during a paced beat. This demonstrates that most nodes followed the same trend as the example electrograms shown in Figure 3. That is, for 80% of heart nodes, the PM selects the MFS for more than 70% of the electrogram.

For each simulated pacing sequence, the mean CC and the mean RE for potentials were computed over all nodes. Figure 5 presents a comparison of the mean CC and mean RE obtained with different methods across the 10 pacing cases. Potentials reconstructed with the PM had higher mean CC and lower mean RE than those reconstructed by MFS and FEM alone ($p < 0.01$). The difference in performance between the PM and MFS was smaller than between the PM and FEM, reflecting the fact the MFS method is selected more often by the PM.

Figures 6 and 7 show two examples of epicardial activation maps during a paced beat, corresponding to potentials directly obtained from the simulation data, or those reconstructed with the MFS, FEM or PM. The black sphere marks the true pacing site location and the white sphere marks the pacing sites detected using each of the different reconstruction methods. In these examples, though the global pattern of activation is similar between the three methods in both cases, key differences exist. The FEM outperformed the MFS in terms of localizing pacing sites (e.g. LE = 5.1

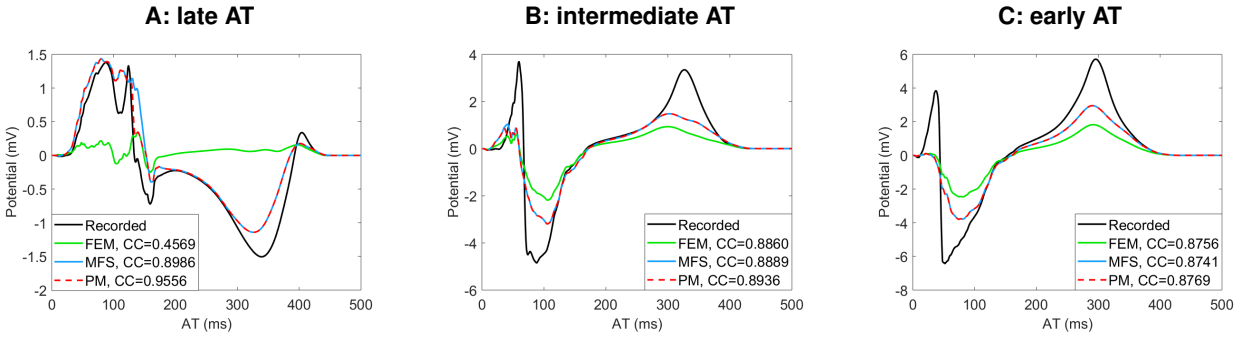

Figure 3: Comparison of simulated and reconstructed electrograms with different methods and their CC during a paced beat. A. At a location with late activation time (AT); B. with intermediate AT; and C. with early AT.

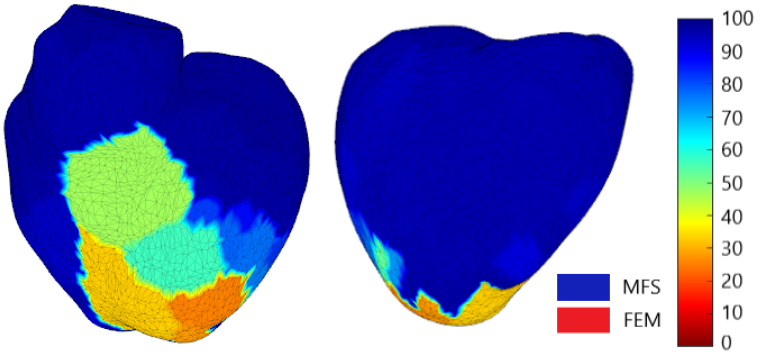

Figure 4: Spatial map demonstrating the percentage of the electrogram each method (FEM or MFS) was selected by the PM during a paced beat.

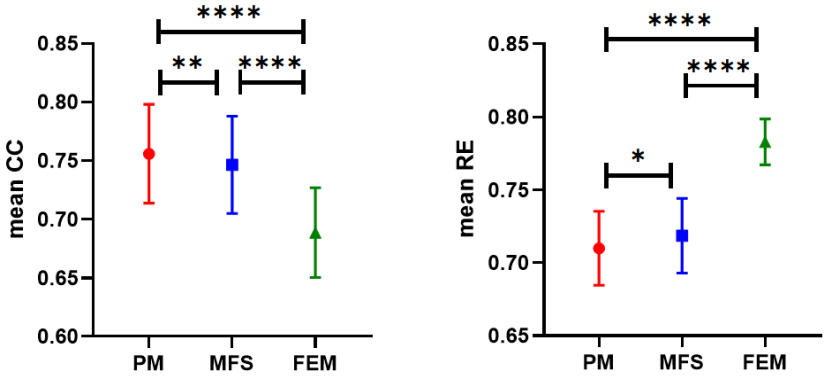

Figure 5: Mean CC and mean RE for paced beats for the PM, MFS and FEM.

and 9.1 mm respectively in Figure 6, although the activation maps were not as smooth as with the MFS particularly in Figure 7. The PM localized the epicardial pacing sites more accurately than either FEM and MFS (LE = 1.5 mm and 4.1 mm in Figures 6 and 7 respectively), and had smoother activation maps than the FEM, though more patchy than the MFS (CC=0.92 and RE=0.14 in Figure 6 and CC=0.84 and RE=0.19 in Figure 7).

Figure 8 shows the CC, RE between activation maps, and the LE of pacing sites for each method for the 10 pacing beats. Activation maps reconstructed by PM showed a higher correlation to the ground truth activation maps than

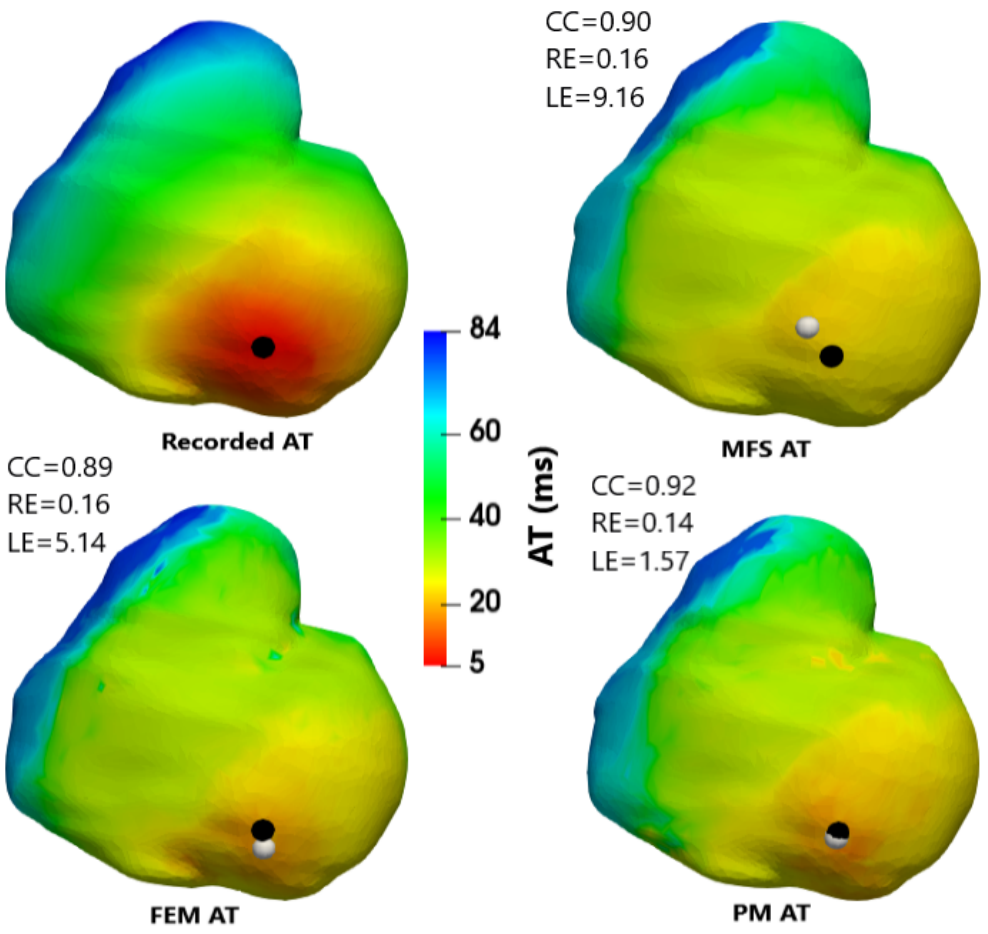

Figure 6: simulated and reconstructed (MFS, FEM and PM) activation times (AT) and pacing localization for a case of left anterior ventricular apical pacing.

those reconstructed by MFS and FEM alone ($p = 0.04$). PM also reduced the RE for activation maps ($p = 0.006$). Though all methods succeeded in capturing the general location of the pacing sites, the LE obtained by the PM was substantially smaller than that obtained by the MFS and FEM ($p = 0.02$). The time differences between ECGI-detected pacing sites and the nearest actual pacing was also smaller for the PM (9.5 ± 7.9) than for the other methods (17.5 ± 9.2 for MFS and 14.2 ± 9.1 for FEM).

3.2. Sinus rhythm

Figure 9 shows examples of simulated and ECGI electrograms during sinus rhythm captured at (A) late, (B) intermediate and (C) early activation sites. As with the pacing sequences, the PM chose the MFS more often than the FEM for the selected electrograms. That is, for 82% of heart nodes the MFS method was selected for more than 70% of the electrogram (figure 10).

For each simulated sinus beat, the mean CC and the mean RE for potentials were computed over all nodes. Figure 11 shows a comparison of the mean CC and mean RE of the different methods across all sinus rhythm data. Potentials reconstructed by PM were more correlated to the measured potentials than those reconstructed by the MFS or the FEM ($p < 0.0001$). PM also reduced the RE for electrograms ($p < 0.0001$).

Figure 12 presents an example of epicardial activation maps in normal sinus rhythm obtained directly from the simulation data as well as reconstructed with the MFS, FEM and PM. The black spheres mark the true breakthrough sites and the white spheres mark the breakthrough sites detected using the MFS, FEM and PM. In this example, the

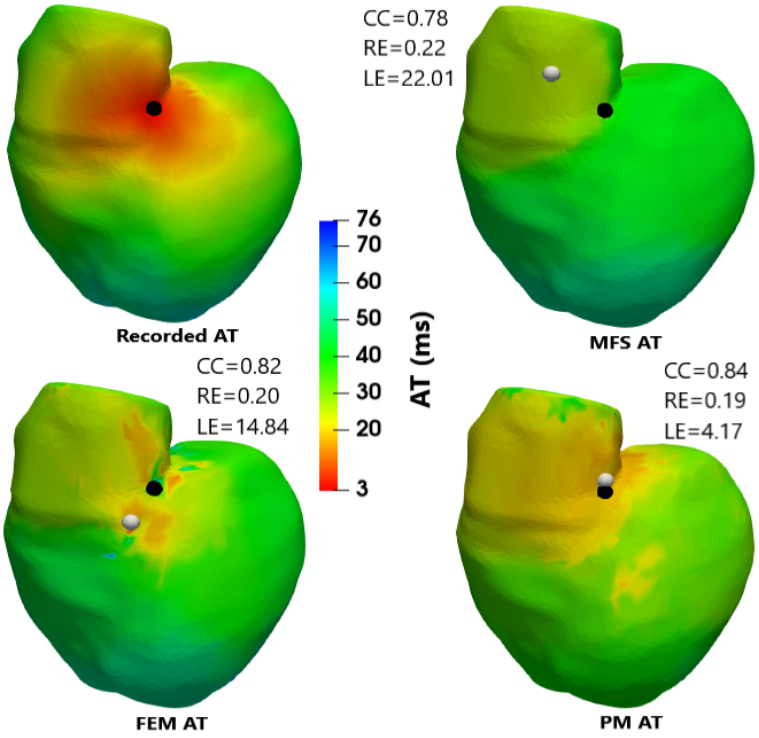

Figure 7: simulated and reconstructed (MFS, FEM and PM) activation times (AT) and pacing localization for a case of pacing on the anterior base. The ventricles are shown in a 45° left anterior oblique view.

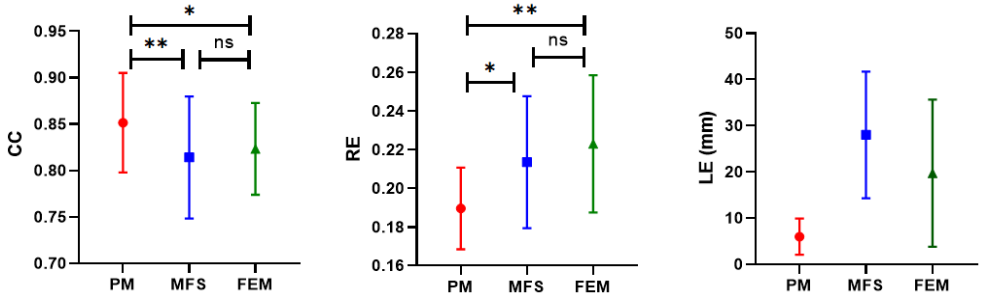

Figure 8: The CC, RE and LE values for activation maps for paced beats for the PM, MFS and FEM.

FEM localized breakthrough sites better than the MFS although, as with pacing data, the activation pattern was less smooth. The PM provided a more accurate activation map pattern (LE1= 18.1, LE2=3.3 and LE3=4.6 mm) than both the FEM and MFS, localizing the epicardial breakthrough sites more accurately than FEM and MFS and having a relatively smooth propagation pattern similar to the simulated pattern (CC=0.50 and RE=0.32).

Figure 13 presents the CC and RE for activation maps with the different methods in sinus rhythm. The PM substantially improved the CC and reduced the RE of activation maps compared to the MFS and FEM ($p < 0.001$).

Table 1 gives a summary of numerical comparisons of ECGI-detected and the nearest true breakthroughs sites. For all sinus rhythm cases, the MFS only captured 2 of the 3 breakthrough sites while the FEM sometimes missed one breakthrough. However the PM always succeeded in detecting all 3 breakthrough sites. The LE obtained by the PM was smaller than that obtained by the FEM and the MFS ($p < 0.0001$) and the time differences between ECGI-detected breakthroughs and the nearest actual breakthrough acquired by the PM were also smaller ($p = 0.04$).

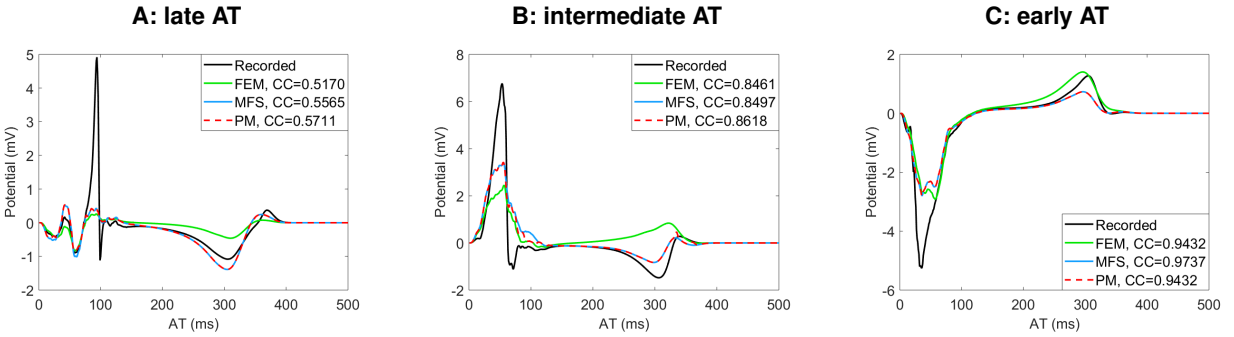

Figure 9: Comparison of simulated and reconstructed electrograms with different methods and their CC during sinus rhythm. A. At a location with late activation time (AT); B. with intermediate AT; and C. with early AT.

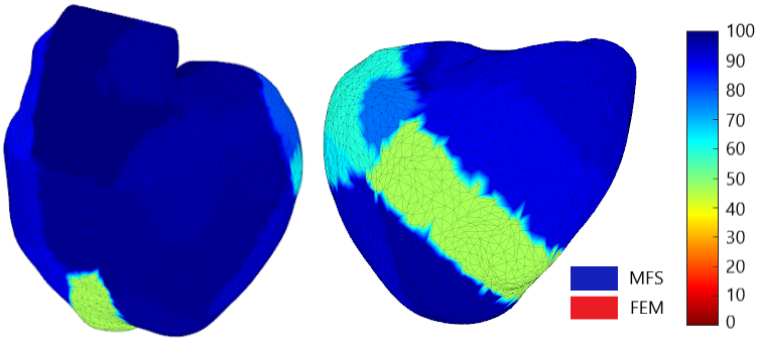

Figure 10: Spatial map demonstrating the percentage of the electrogram each method (FEM or MFS) was selected by the PM during sinus rhythm.

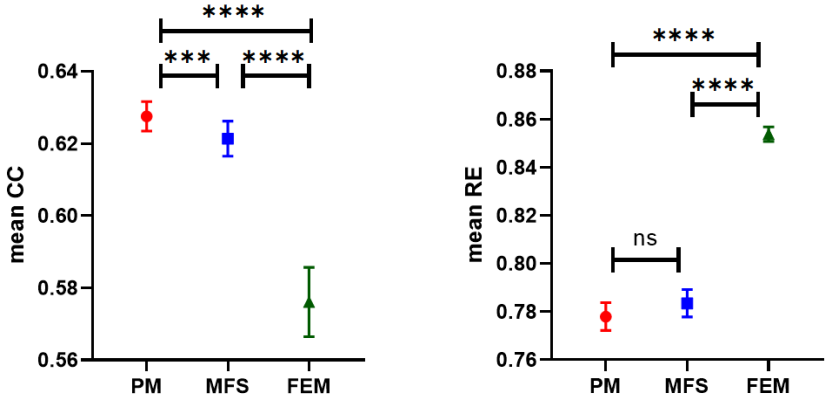

Figure 11: The mean CC and mean RE for potentials in sinus rhythm for the PM, MFS and FEM.

3.3. Effect of noise

3.3.1. Pacing

Figure 14 shows a comparison of the mean CC and mean RE values for potentials (panel A and panel B respectively) as well as CC and RE values for activation times (panel C and panel D respectively) obtained with the different reconstruction methods across the entire pacing data set at different noise levels. All of the methods are sensitive to noise with CC decreasing (panel A) and RE increasing (panel B) with higher noise levels. Despite this sensitivity,

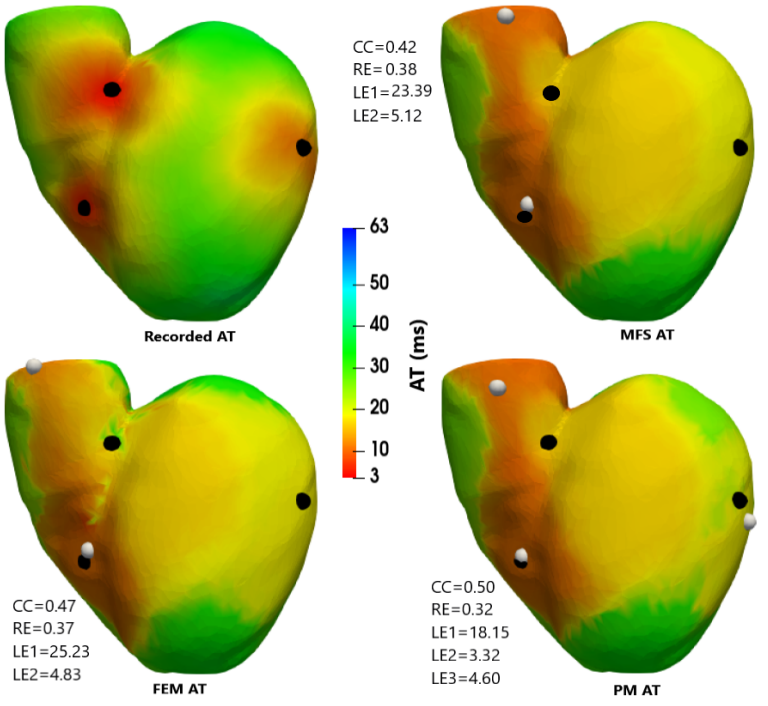

Figure 12: simulated and reconstructed (MFS, FEM and PM) activation times (AT) and breakthrough localization during sinus rhythm.

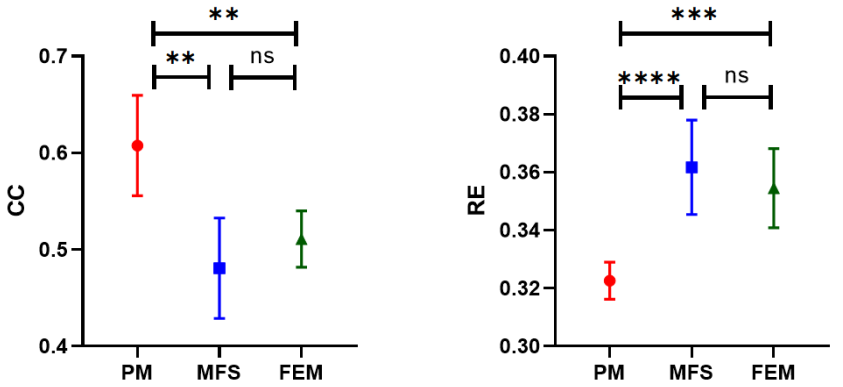

Figure 13: Correlation coefficients (CC) and relative errors (RE) for activation time for PM, MFS and FEM in sinus rhythm.

potentials reconstructed with PM showed higher CC and lower RE to the true potentials than those reconstructed by MFS and FEM at all noise levels ($p < 0.0001$). Furthermore, the reduction in CC and increase in RE with each noise level was smaller for the PM than for the MFS and FEM, demonstrating it was less sensitive to the addition of noise. For activation maps, as was seen with the reconstructed potentials, the accuracy of the reconstructed activation maps is reduced with increasing noise levels. Likewise, activation maps reconstructed by the PM show a higher CC (panel C) and lower RE (panel D) to the ground truth activation maps than those reconstructed by MFS and FEM at all noise levels ($p < 0.0001$). The PM again minimized the increase and reduction in RE and CC respectively compared to the FEM and MFS.

		MFS	FEM	PM
N_{BT}	actual	3	3	3
	detected	2	2–3	3
LE (mm)	LE1	20.5±5.4	22.2±4.7	15.7±3.6
	LE2	5.0±1.2	7.9±3.6	4.9±1.7
	LE3			3.3±1.5
time offset (ms)	1	5.9±0.0	5.9±0.0	4.7±0.0
	2	5.7±0.0	5.2±0.0	4.8±0.0
	3			8.3±0.0

Table 1
Numerical comparisons of ECGI-detected and true epicardial breakthrough sites. N_{BT} = number of breakthroughs.

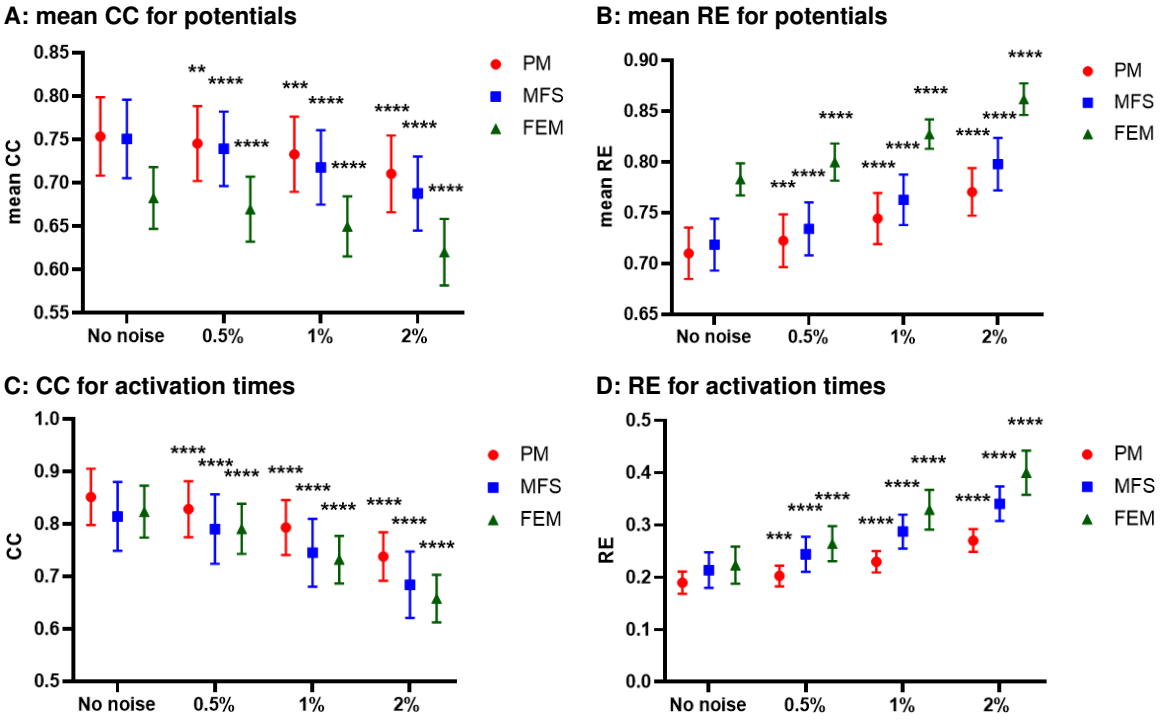

Figure 14: Comparison of CC and RE for potentials and activation maps for paced beats for the PM, MFS and FEM after adding different levels of noise. A. mean CC for potentials; B. mean RE for potentials; C. CC for AT; and D. RE for AT.

3.3.2. Sinus rhythm

Figure 14 presents a comparison of the mean CC and mean RE values for potentials (panel A and panel B respectively) as well as CC and RE values for activation times (panel C and panel D respectively) computed for each sinus rhythm simulation for the different reconstruction methods at different noise levels added to the body surface potential distribution. Despite the sensitivity of the methods to noise, potentials reconstructed with the PM showed higher CC (panel A) and lower RE (panel B) than those reconstructed by MFS and FEM. Furthermore, the degradation in RE with the PM was small compared to the FEM and MFS. For the activation maps in sinus rhythm reconstructed with the different methods over all noise levels, as with the potentials, at all noise levels the PM reconstructed activation maps with higher CC (panel C) and lower RE (panel D) than the other methods. Moreover the reduction in CC and increase in RE MFS or FEM was larger with increasing noise level than was seen with the PM .

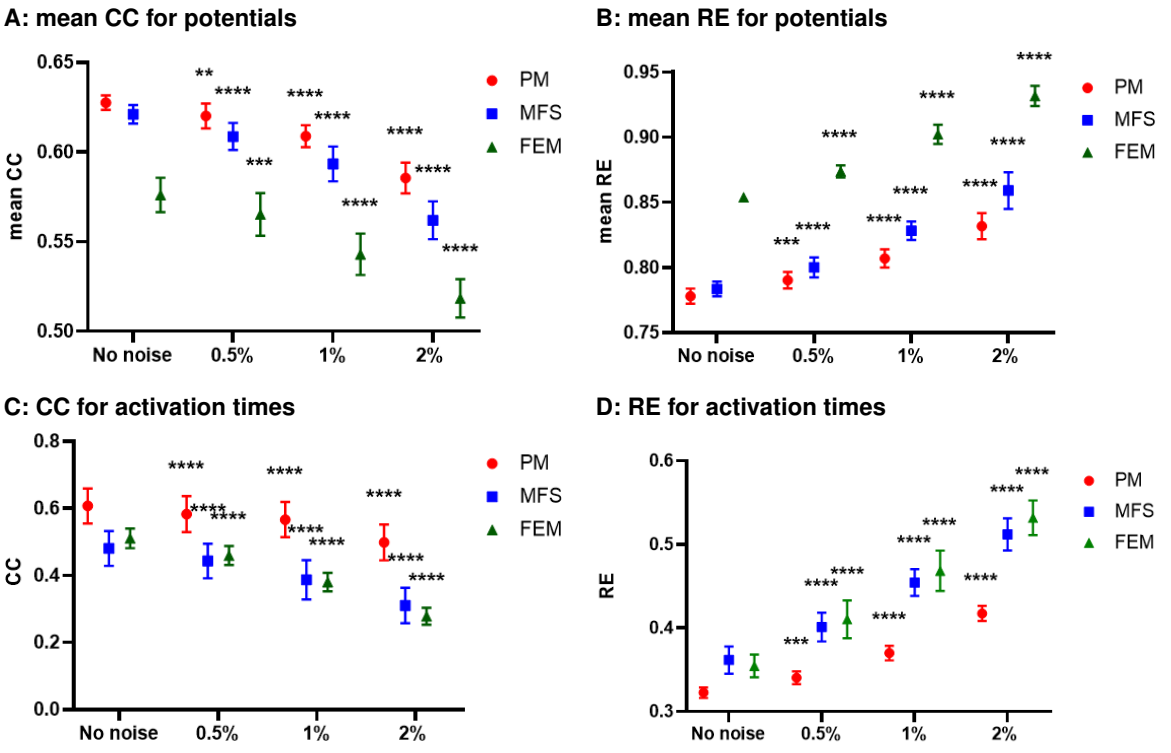

Figure 15: Comparison of CC and RE for potentials and activation maps during sinus rhythm for the PM, MFS and FEM after adding different levels of noise. A. mean CC for potentials; B. mean RE for potentials; C. CC for AT; and D. RE for AT.

4. Discussion

We presented an innovative ECGI method to improve the accuracy of reconstructed epicardial electrical activity. This novel approach, called the Patchwork Method (PM), combines the solutions obtained with two classic ECGI numerical methods (FEM and MFS), using another classic numerical approach, the BEM, to compare their residuals in order to select the most accurate method.

We have demonstrated that the FEM performs globally better than the MFS for localizing pacing sites and epicardial breakthroughs in sinus rhythm, while for the accuracy of the potential reconstruction the MFS performs better. By combining the FEM and MFS solutions into the PM solution we obtained better results than for either method alone, even outperforming the FEM and the MFS where they each perform best. Interestingly, the improvement obtained with the PM for activation times was most significant in sinus rhythm, which is more difficult to reconstruct than paced beats. This study is to our knowledge the first one to discuss results using different numerical methods in the case of sinus rhythm. Finally, we demonstrated the stability and robustness of the PM to Gaussian measurement noise added to the body surface potential distribution, with the PM consistently out-performing the other methods.

Since the inverse problem of electrocardiography was first described over 50 years ago, many novel methods to solve it have been developed; including numerical methods for the forward problem [9, 8, 7], regularization techniques [20, 21, 10] and methodologies to compute the regularization parameter [12, 14, 22]. Several studies have aimed to compare these various methods in order to determine an optimal approach [12, 13, 11]. But as the number of new methods grows, the number of possible combinations of the different methods also expands. For example, in one of these most recent studies [11], two different numerical approaches were combined with two different regularization methods, and five different methods to compute the regularization parameter resulting in fifteen different inverse problem pipelines. Furthermore, there appears to be no single best approach. Rather, the optimal methods depends not only on the data set or activation sequence [11], but also the level of noise [12, 13] and the geometric error present in the data [13]. One advantage of the PM is therefore in its versatility: that is its potential to combine the results based on any ECGI method, including MFS and FEM, with various regularization parameters to always provide the optimal solution regardless of

the data used, or noise/geometric error present.

The idea of combining numerical methods to solve the inverse problem of electrocardiography has previously been suggested. Bradley et al. [23] built a new model by coupling the FEM and BEM (F-BEM) in order to construct the transfer matrix. F-BEM models use the BEM for isotropic and homogeneous regions of the torso (e.g., the lungs and the torso cavity), and the FEM for anisotropic zones (e.g., the skeletal muscle). The main advantage of this coupled model is to use the appropriate modeling technique in the appropriate region. This reduces the overall size of the problem, while still allowing the model to be refined in areas of high gradients (i.e. around the heart), without the need to have the same mesh density propagated to areas with low gradients (e.g. the outer torso surface). Though this overcomes several limitations of the individual numerical methods, the model will still result in a single inverse solution with a performance that will depend on the factors presented above.

Optimizing the inverse solution based on minimizing the torso residual has also previously been proposed. Bergquist et al. [24] have proposed improving ECGI accuracy with a geometric correction method. This method minimized the cardiac geometry localization error by reducing errors from respiratory movement. To improve the localization of the heart and the ECGI accuracy they used an iterative coordinate descent optimization. A single inverse solution was calculated in each iteration with current per-beat estimates of cardiac location using BSPs from multiple beats. The solution was then used to estimate new cardiac positions for each beat by minimizing forward solution error.

One of the limitations of our work is the use of simulated data. Although we added Gaussian noise, other real-word sources of error were not evaluated and require validation using experimental or clinical data. We expect that the accuracy of the PM using clinical data will not be better than in the case of simulation data, due to the presence of geometric error and other uncertainties. However, as we take the best method in each zone and at each time step, we expect that even in the case of experimental or clinical data the PM will improve the reconstruction of the electrical potentials and activation times on the heart compared to classic ECGI approaches.

The PM implementation presented uses a single regularization method (zero-order Tikhonov) and a single method to define the regularization parameter (CRESO). Previous studies have demonstrated the dependence of reconstruction accuracy on both regularization method and parameter selection methods, with the optimal method depending on the numerical method chosen. For example, Karoui et al. [11] demonstrated a variability in CC and RE of up to 30% for a single numerical method, depending on the regularization parameter selection method used. An advantage of the PM approach is that it is theoretically unlimited in the number of methods that could be combined and optimized. We will therefore work in the future to incorporate different regularization and parameter selection methods into the PM workflow.

5. Conclusion

We presented a novel ECGI approach to reconstruct cardiac electrical activity that optimizes reconstruction accuracy by selecting the best reconstruction method for each node and time step. This new approach, called the Patchwork Method, is an efficient tool to help overcome some of the limitations of current numerical methods, improving the accuracy of reconstructed potential and activation maps and the localization of epicardial breakthroughs during pacing and sinus rhythm. By ensuring the optimal solution is always reconstructed, this new approach may be useful in determining the limits in accuracy of previously developed ECGI approaches based on epicardial sources.

Funding sources

This work was supported by the French National Research Agency, grant reference ANR-10-IAHU04-LIRYC. This work was granted access to the HPC resources of CINES under the allocation 2020-A0070307379 made by GENCI

References

[1] L. R. Bear, P. R. Huntjens, R. D Walton, O. Bernus, R. Coronel, and R. Dubois. Cardiac electrical dyssynchrony is accurately detected by noninvasive electrocardiographic imaging. *Heart Rhythm*, 15:1058–1069, 2018.

[2] S. Ploux, J. Lumens, Z. Whinnett, M. Montaudon, M. Strom, C. Ramanathan, N. Derval, A. Zemmoura, A. Denis, M. De Guillebon, A. Shah, M. Hocini, P. Jaïs, P. Ritter, M. Haïssaguerre, L. B. Wilkoff, and P. Bordachar. Noninvasive electrocardiographic mapping to improve patient selection for cardiac resynchronization therapy. *J. Am. Coll. Cardiol.*, 61:2435–2443, 2013.

[3] M. Haissaguerre, M. Hocini, A. Denis, A. J. Shah, Y. Komatsu, S. Yamashita, M. Daly, S. Amraoui, S. Zellerhoff, M. Picat, A. Quotb, L. Jesel, H. Lim, S. Ploux, P. Bordachar, G. Attuel, V. Meillet, P. Ritter, N. Derval, F. Sacher, O. Bernus, H. Cochet, P. Jais, and R. Dubois. Driver domains in persistent atrial fibrillation. *Circ*, 130:530–538, 2014.

[4] L. R. Bear, O. Bouhamama, M. Cluitmans, J. Duchateau, R. D. Walton, E. Abell, C. Belterman, M. Haissaguerre, O. Bernus, R. Coronel, and R. Dubois. Advantages and pitfalls of noninvasive electrocardiographic imaging. *J. Electrocardiol.*, 57, 2019.

[5] J. Duchateau, F. Sacher, T. Pambrun, N. Derval, J. Chamorro-Servent, A. Denis, S. Ploux, M. Hocini, P. Jaïs, O. Bernus, M. Haïssaguerre, and R. Dubois. Performance and limitations of noninvasive cardiac activation mapping. *Heart Rhythm*, 16:435–442, 2018.

[6] J. L. Sapp, F. Dawoud, J. C. Clements, and B. M. Horácek. Inverse solution mapping of epicardial potentials: quantitative comparison with epicardial contact mapping. *Circ. Arrhythm. Electrophysiol.*, 5:1001–1009, 2012.

[7] R. C. Barr, M. Ramsey, and M. S. Spach. Relating epicardial to body surface potential distributions by means of transfer coefficients based on geometry measurements. *IEEE Trans. Biomed. Eng.*, 24:1–11, 1977.

[8] P. Colli-Franzone, L. Guerri, B. Taccardi, and C. Viganotti. Finite element approximation of regularized solutions of the inverse potential problem of electrocardiography and applications to experimental data. *Calcolo. Springer*, 22:91–186, 1985.

[9] Y. Wang and Y. Rudy. Application of the method of fundamental solutions to potential-based inverse electrocardiography. *Ann. Biomed. Eng.*, 34:1272–1288, 2006.

[10] A. Tikhonov and V. Arsenin. *Solution of ill-posed problems*. John Wiley & Sons, Washington, D.C., 1977.

[11] A. Karoui, L. Bear, P. Migerditichan, and N. Zemzemi. Evaluation of fifteen algorithms for the resolution of the electrocardiography imaging inverse problem using ex-vivo and in-silico data. *Front Physiol*, 9, 2018.

[12] P. R. Johnston and R. M. Gulrajani. A new method for regularization parameter determination in the inverse problem of electrocardiography. *IEEE Trans. Biomed. Eng.*, 44:19–32, 1997.

[13] L. K. Cheng, J. M. Bodley, and A. J. Pullan. Comparison of potential- and activation-based formulations for the inverse problem of electrocardiology. *IEEE Trans. Biomed. Eng.*, 50:11–22, 2003.

[14] P. Colli-Franzone, L. Guerri, S. Tentoni, C. Viganotti, S. Baruffi, S. Spaggiari, and B. Taccardi. A mathematical procedure for solving the inverse potential problem of electrocardiography. analysis of the time-space accuracy from in vitro experimental data. *Math. Biosci.*, 77:353–396, 1985.

[15] M. Kania, Y. Coudière, H. Cochet, P. Jaïs, and M. Potse. Prediction of the exit site of ventricular tachycardia based on different ECG lead systems. In Christine Pickett, Cristiana Corsi, Pablo Laguna, and Rob MacLeod, editors, *Computing in Cardiology*, volume 44, Rennes, France, 2017.

[16] K. H. W. J. ten Tusscher, D. Noble, P. J. Noble, and A. V. Panfilov. A model for human ventricular tissue. *Am. J. Physiol. Heart Circ. Physiol.*, 286:H1573–H1589, 2004.

[17] M. Potse. Scalable and accurate ECG simulation for reaction-diffusion models of the human heart. *Front. Physiol.*, 9:370, 2018.

[18] M. G. Hoogendijk, M. Potse, A. C. Linnenbank, A. O. Verkerk, H. M. den Ruijter, S. C. M. van Amersfoorth, E. C. Klaver, L. Beekman, C. R. Bezzina, P. G. Postema, H. L. Tan, A. G. Reimer, A. C. van der Wal, A. D. J. ten Harkel, M. Dalinghaus, A. Vinet, A. A. M. Wilde, J. M. T. de Bakker, and R. Coronel. Mechanism of right precordial ST-segment elevation in structural heart disease: Excitation failure by current-to-load mismatch. *Heart Rhythm*, 7:238–248, 2010.

[19] J. Duchateau, M. Potse, and R. Dubois. Spatially coherent activation maps for electrocardiographic imaging. *IEEE Trans. Biomed. Eng.*, 64:1149–1156, 2017.

[20] G. Shou, L. Xia, M. Jiang, Q. Wei, F. Liu, and S. Crozier. Truncated total least squares: a new regularization method for the solution of ECG inverse problems. *IEEE Trans. Biomed. Eng.*, 55:1327–35, 2008.

[21] F. Greensite. A new method for regularization of the inverse problem of electrocardiography. *Math. Biosci.*, 111:131–54, 1992.

[22] P. C. Hansen. *Rank-deficient and discrete ill-posed problems: Numerical aspects of linear inversion*. SIAM, Philadelphia, PA, 1998.

[23] C. P. Bradley, A. J. Pullan, and P. J. Hunter. Geometric modeling of the human torso using cubic Hermite elements. *Ann. of Biomed. Eng.*, 25(1):96–111, 1997.

[24] J. A Bergquist, J. Coll-Font, B. Zenger, L. C. Rupp, W. W. Good, D. H. Brooks, and R. S. MacLeod. Improving localizing cardiac geometry using ECGI. Comp. in Cardiol., 2020.